NANO LETTERS

Letter

A Semiconductor Exciton Memory Cell Based on a Single Quantum Nanostructure

Hubert J. Krenner, Craig E. Pryor, Jun He, and Pierre M. Petroff

Nano Lett., **2008**, 8 (6), 1750-1755 • DOI: 10.1021/nl800911n • Publication Date (Web): 24 May 2008

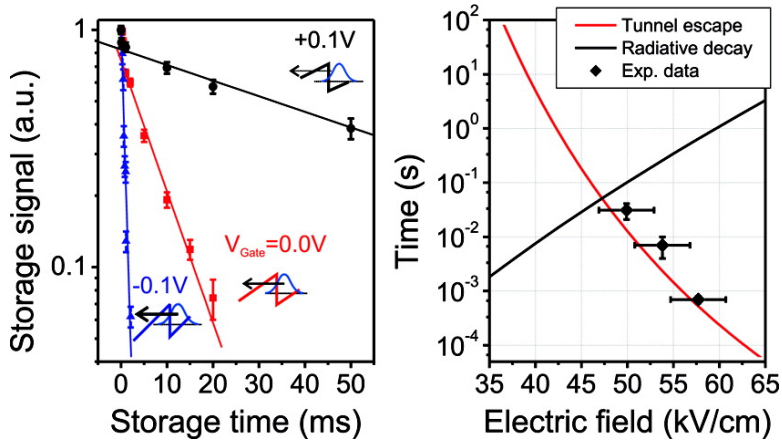

More About This Article

Additional resources and features associated with this article are available within the HTML version:

- Supporting Information
- Links to the 1 articles that cite this article, as of the time of this article download
- Access to high resolution figures
- Links to articles and content related to this article
- Copyright permission to reproduce figures and/or text from this article

View the Full Text HTML

NANO LETTERS

2008
Vol. 8, No. 6
1750-1755

A Semiconductor Exciton Memory Cell Based on a Single Quantum Nanostructure

Hubert J. Krenner,*,† Craig E. Pryor,‡ Jun He,† and Pierre M. Petroff†

Materials Department, University of California, Santa Barbara, California 93106, and Department of Physics and Astronomy, University of Iowa, Iowa City, Iowa 52242

Received April 1, 2008; Revised Manuscript Received May 12, 2008

ABSTRACT

We demonstrate storage of excitons in a single nanostructure, a self-assembled quantum post. After generation, electrons and holes forming the excitons are separated by an electric field toward opposite ends of the quantum post inhibiting their radiative recombination. After a defined time, the spatially indirect excitons are reconverted to optically active direct excitons by switching the electric field. The emitted light of the stored exciton is detected in the limit of a single nanostructure and storage times exceeding 30 msec are demonstrated. We identify a slow tunneling of the electron out of the quantum post as the dominant loss mechanism by comparing the field dependent temporal decay of the storage signal to models for this process and radiative losses.

The zero-dimensional density of states of self-assembled semiconductor quantum dots (QDs) provides the basis for numerous applications for novel optoelectronic devices such as optical modulators and low-threshold lasers[1] and also allows studying fundamental physical phenomena in these nanostructures. In particular, spins[2–4] and excitons[5–8] have been of interest for implementing quantum computation and communication schemes[9] in the solid state. Indeed, self-assembled QDs are inherently scalable[10,11] and can be addressed, manipulated, and read out both electrically and optically.[3,4,6,12] Recently, memory devices based on QDs[3,13,14] have been realized and spin-to-photon conversion has been demonstrated.[3] However, in these experiments one carrier initially forming the exciton is lost to a reservoir, resulting in the loss of phase information. Here, we report the storage of optically or electrically generated excitons in a novel type of nanostructure: a self-assembled quantum post (QP).[15] Unlike in QD based approaches, in our system, both electrons and holes remain localized within the same nanostructure in which they are generated, maintaining the phase between the electron and the hole. By applying an electric field along the QP axis, electrons and holes are spatially separated toward opposite ends of the QP. This results in a large electrostatic dipole moment and a large increase in the radiative lifetime of the exciton. Such stored excitons can be reconverted into photons simply by switching a gate voltage after a defined time. The storage time exceeds 30 ms at 7 K and is only limited by electron tunnelling out of the QP. These timescales are sufficiently long to study the mutual electron−hole spin coherences and reconversion from stationary to flying photonic qBITs using our storage scheme. In addition, the large and tunable electrostatic dipole moment of the stored exciton gives rise to a pronounced change of the dielectric properties and tailored optical nonlinearities. This could find direct application in optical phase modulation devices with superior performance.

The novel nanostructure used in these experiments is a self-assembled quantum post[15,16] which is a short quantum wire with a QD at each end and is embedded in a semiconductor matrix. In contrast to well-established self-assembled QDs, the height of the QP can be controlled with nanometer precision up to 60 nm, and the aspect ratio can be engineered. The QPs are embedded in a shallow quantum well preserving confinement in the lateral direction. A detailed description of the QP fabrication and the device can be found in Supporting Information. In contrast to quantum wells,[17,18] in our system, individual excitons are fully localized within a single nanostructure and strongly decoupled from the environment. The controllable height and large aspect ratio allows for charge separation along the QP axis while keeping the electron and hole localized within the same nanostructure. This property is required for the generation and phase preserving storage of indirect excitons and their reconversion into photons which we demonstrate in this paper. Unlike single or coupled QD based approaches,

* Corresponding author. E-mail: krenner@engineering.ucsb.edu.
† University of California.
‡ University of Iowa.

10.1021/nl800911n CCC: $40.75
Published on Web 05/24/2008

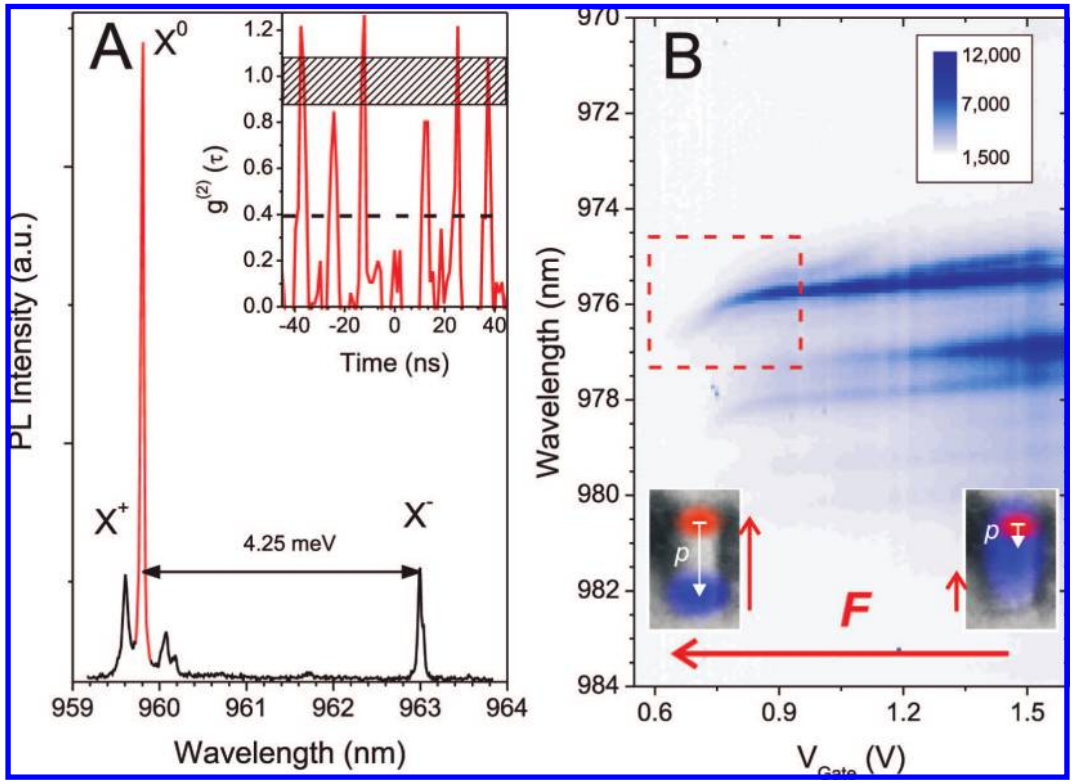

Figure 1. Characterization of individual QPs. (a) Micro-PL spectrum of a single QP with an autocorrelation histogram (inset) for the neutral exciton (X^0, marked in red). $T = 7$ K and $P_0 = 1$ W/cm^{-2}. As expected for a single photon source, the peak at $\tau = 0$ ns is clearly reduced compared with the average peak height (shaded bar) indicative for a single quantum emitter. (b) Transition from direct to indirect excitons observed in the photoluminescence spectrum of a single QP under applied bias voltage at $T = 7$ K and $P_0 = 50$ W/cm^{-2}. For decreasing gate potential, the electron−holes pairs get spatially separated by the increase of the applied electric field as shown schematically. At $V_{Gate} \sim 0.6$ V, the carrier overlap vanishes, and the emission quenches which is accompanied by a change of the shift rate due to the QCSE. The small inserts correspond to a cross section TEM of a QP with the electron and hole wave functions schematically added to it.

our scheme should allow for full transfer of quantum information from a stationary spin or exciton back into the optical domain of a flying photonic qBIT[19].

We begin with introducing the fundamental optical properties of QPs. In Figure 1a, we show a typical micro-photoluminescence (PL) spectrum recorded from an individual 40 nm high QP under low optical excitation. This QP is not embedded in an electrically active structure, and therefore, no electric field is applied. The spectrum shows three dominant lines corresponding to the QP exciton ground-state shell which can be attributed to recombination of the neutral exciton ($X^0 = 1e + 1h$, marked in red) and two charged excitons ($X^+ = 1e + 2h$ and $X^- = 2e + 1h$). The energy splitting between these different charge states is comparable to self-assembled quantum dots[11,16] (e.g., X^- is shifted by 4.25 meV to lower energy compared with X^0). We recorded the autocorrelation function $g^{(2)}(\tau)$ of the X^0 line under pulsed excitation (inset of Figure 1a). In the typical periodic pattern, the peak at $\tau = 0$ s measures the probability for emission of two photons per excitation cycle. It is clearly suppressed well below the average height of the other peaks marked by the shaded gray bar providing direct evidence that QPs are efficient single photon emitters.[7] In particular, a single quantum emitter is required for efficient conversion between exciton or spin excitations and photons, that is, between stationary and flying qBITs.[19]

In a second experiment, we studied the influence of a static electric field (F) on the QP emission. The underlying tuning mechanism is the quantum confined Stark effect (QCSE) which has proven to be a particularly powerful tuning mechanism to manipulate, read, or couple qBITs in quantum dots.[5,10−12] Figure 1b shows micro-PL spectra of an individual 40 nm QP encoded in the color scale as a function of the wavelength and the gate potential (V_{Gate}) applied to our device (see Supporting Information). F is oriented along the QP axis and increases with decreasing V_{Gate} as shown schematically in Figure 1b. For low electric fields ($V_{Gate} \sim$ 1.4 V), we observe two dominant spectral lines which originate from recombination of neutral and charged excitons in the QP. As F increases, all lines show a weak shift due to the QCSE up to $V_{Gate} = \sim$0.8 V. At this voltage, the PL energy rapidly changes, and its intensity quenches. Tunneling of carriers is not expected at such fields ($F \sim 30$ kV/cm) and cannot explain the change in the QCSE. The magnitude of the Stark shift is given by $\Delta E_{Stark} = p \cdot \Delta F$, where p is the static excitonic dipole moment. It is directly related to the mean distance of the electron and hole wave functions $s_{e\text{-}h}$ via $p = e \cdot s_{e-h}$ with e being the elementary charge.[10] For $V_{Gate} > 0.9$ V, the electron and hole are strongly bound via their mutual Coulomb interaction, and therefore, $s_{e\text{-}h}$ remains small and almost constant giving rise to a weak shift rate. For $V_{Gate} < 0.9$ V, the Stark shift ΔE_{Stark} becomes the dominant energy

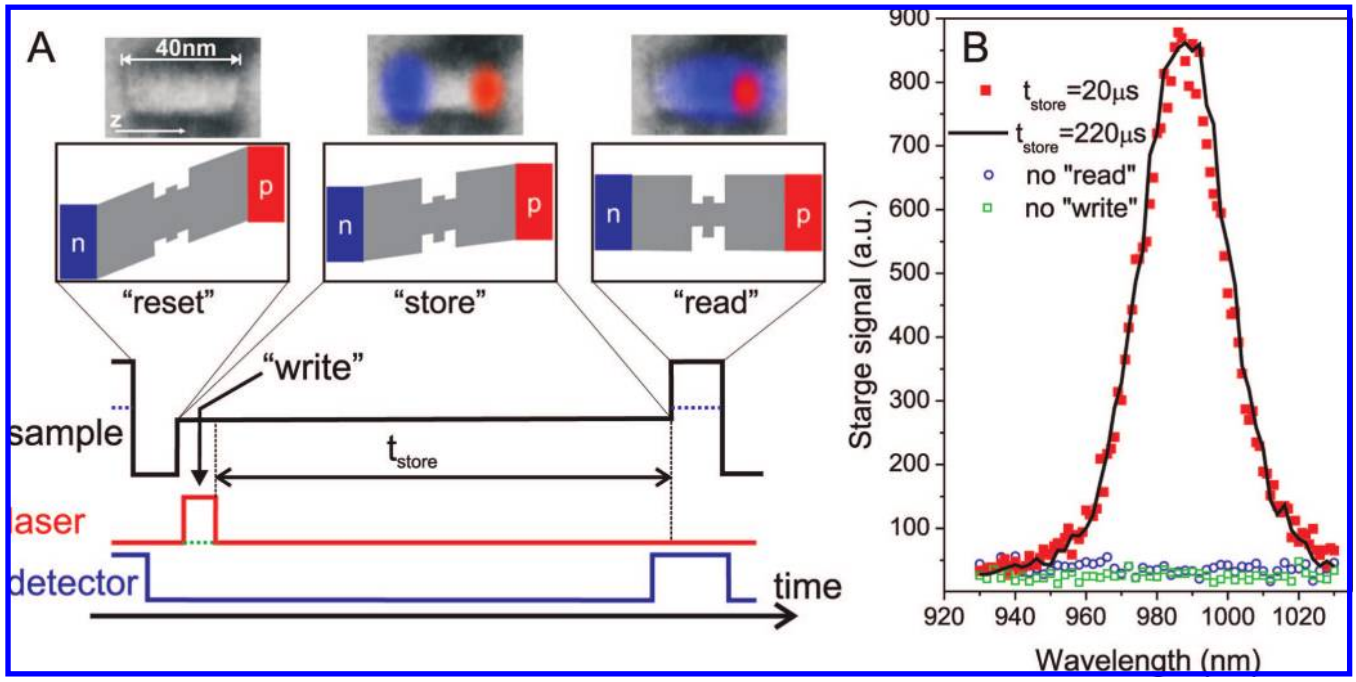

Figure 2. Storage of indirect excitons in QPs. (a) Schematic of the storage scheme. After a reset step during which the QP is emptied, the sample voltage (black) is switched to the indirect exciton regime. In the beginning of the storage, interval electrons and holes are written by a laser (red) into the QP and after $t_{storage}$ read via direct excitons. The detection (blue) is activated only during the time the read step. The bandstructure and spatial carrier distribution during each step are shown schematically. For control experiments, the write and read pulses are turned off individually as shown by the dashed lines. (b) Storage spectra taken from a QP ensemble after 20 μs (full squares) and 200 μs (line) storage times ($P_{exc} = 20$ kW/cm^{-2}, $T = 7$ K). Without the write and read pulses (open symbols) no signal is detected proving the storage principle.

contribution and exceeds the binding energy. Therefore, the electron and hole are separated by the electric field, and their distance increases, resulting in a larger value of p which is limited by the height of the QP. This increase in p results in a much larger slope of the Stark shift and a quenching of the PL intensity due to a drastic decrease in oscillator strength. This transition is more abrupt for larger QP height, and the slope of the indirect exciton is not resolvable. However, for shorter QPs, this asymptotic linear shift is observed[16] and an example of a 23 nm high QP is included as Supporting Information Figure S1. The resolved transition to a linear slope directly reflects the spatial separation of electron and hole. Moreover, the electrostatic dipole moment of $p = e$•20 nm determined from the slope reflects the QP height. The linear shift reflecting the QP height, the reduction of the oscillator strength, and the lateral carrier confinement are due to the unique electronic properties of QPs which in contrast to conventional quantum well or QD structures can be accurately tailored. Furthermore, these two observations provide a clear, characteristic fingerprint for an electric field-driven separation of individual electrons and holes within the QP leading to a spatially indirect exciton whose radiative lifetime is substantially and controllably increased.

This unique QCSE enables us to implement a scheme for storing an indirect exciton in a QP as shown schematically in Figure 2a. Our method uses a sequence of three electrical pulses for gating: the sample, the laser to write excitons, and the detector to read the stored signal. For each step, the spatial distribution of the electron and hole and the band structure are depicted schematically. The storage sequence starts with a reset step under a large reverse bias ($V_{reset} \sim -5$ V) under which carriers can tunnel out of the QP. In the next step, the sample bias is raised to V_{store}, a level where the exciton is in a spatially indirect long-lived state while carrier tunnelling out of the QP is suppressed. At the start of this storage interval, the laser is turned on for 500 ns to write photogenerated electrons and holes into the QPs. During storage, both carriers are localized in the same nanostructure but remain spatially separated because of the applied electric field. When the sample bias is brought back close to flat-band (V_{read}) for a time $t_{read} = 1$ μs, the stored excitons become spatially direct. Under these conditions, the electron and hole wave functions overlap, and radiative recombination can occur. The emitted photons are then detected during this read step. To reduce the dark count level, the detector is read out only while the read voltage is applied. Thus, we define the storage time (t_{store}) as the difference between the time when the "write" laser is turned off and the time a "read" voltage is applied.

To demonstrate this scheme, we used a sample with a low surface density of QPs ($\sim$1000/μm^2). The store and read voltages were set to $V_{store} = +0.5$ V and $V_{read} = +1.5$ V, respectively. Typical storage spectra as a function of wavelength are shown in Figure 2b for $t_{store} = 20$ μs and 220 μs. We find a pronounced peak centered at $\lambda = 987$ nm with a width of 34 nm consistent with the QP ground-state PL for a QP ensemble.[15] The intensity of this storage peak does not decrease when the storage time is increased by more than an order of magnitude demonstrating loss-free storage of excitons. Higher excitation densities are required for

storage compared with PL experiments (e.g., shown in Figure 1) since at these voltages the carrier capture is significantly quenched. The levels used were chosen a factor ~10 higher than the excitation density at which the onset of the storage signal is observed. We want to note that, because of the nonresonant nature of the excitation, we cannot exclude that charged excitons are contributing to the storage signal. Since the excitation densities are not significantly increased beyond the observed onset, multiexcitons (bi- or triexcitons) should still be negligible.

Two control experiments were performed to demonstrate that we are indeed storing an indirect exciton. In the first one, the read voltage is set to a level at which the exciton ground-state remains indirect. For this condition, we do not expect to detect a stored signal since radiative recombination strongly suppressed for indirect excitons. To confirm that the read signal originates from excitons photogenerated by the write laser and not from carriers, respectively, from two individual electrically injected from the doped layers, a second control experiment was done in which the laser remains off. No storage signal should be detected even though the read voltage is applied since no excitons were written. The results of these two control experiments are shown as blue (no read) and green (no write) symbols for $t_{store} = 20\ \mu s$ in Figure 2b. Clearly, no signal is detected in both cases demonstrating that we store excitons in the QPs, which are later read-out simply by changing the gate potential on our device.

In another experiment, we extended our storage scheme down to the limit of a single QP. We recorded storage signals of $1.1 \pm 0.1 \times 10^{-4}$ and $4.8 \pm 0.5 \times 10^{-4}$ counts/cycle, after storage times of 20 μs and 30 μs, respectively, from two individual QPs (spectra shown in Supporting Information Figure S2). Since only a single QP is addressed, a reduced excitation power densities ($P_{exc} = 100\ W/cm^{-2}$) is used. To avoid monochromator losses, the emission of the QPs was detected after spectral filtering using a 10 nm bandpass filter centered at the single QP main emission line as shown in Supporting Information Figure S2. In the control experiments without the write or read step, we measured a background of $0.7 \pm 0.1 \times 10^{-4}$ and $2.0 \pm 0.5 \times 10^{-4}$ counts/cycle for the two QPs. From these values, we obtain net storage signals of $0.4 \pm 0.2 \times 10^{-4}$ and $2.8 \pm 1 \times 10^{-4}$ counts/cycle. These values agree well with the expected, instrumentation limited signal strength from a single QP of $\sim 10^{-4}$ counts/cycle. The higher count rate for 30 μs storage time compared with that of 20 μs is associated with differences in the alignment which are most pronounced at these low count rates. As shown in Figure 2, losses do not occur for times exceeding 200 μs and, therefore, can be excluded. The detected contrast between the full storage scheme and the control experiments clearly demonstrates that even the weak storage signal of a single QP can be detected without using microcavity structures. In Figure 3a we plot the integrated storage signal as a function of $t_{storage}$ for three different values of $V_{storage}$. For $V_{storage} = +0.1$ V ($F \sim 50$ kV/cm), we observe a slow exponential decay of the storage signal with a time constant of 30 ± 7 ms. As $V_{storage}$ is lowered and the electric field is

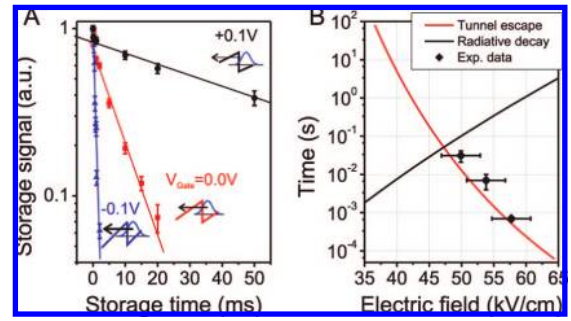

Figure 3. Temporal decay of the storage signal and identification of loss mechanism. (a) For increasing reverse bias (increasing electric field), the storage signal decays over time due to tunnel escape of electrons from the QPs as shown schematically. (b) Comparison between experimentally observed decay times (symbols) and calculated tunnelling time (red line) using a WKB approximation and radiative lifetime (black line) as a function of F demonstrates that tunnelling is the dominant loss mechanism.

increasing, we observe faster decays with 7 ± 1 ms and 0.7 ± 0.2 ms for 0.0 V ($F \sim 54$ kV/cm) and -0.1 V ($F \sim 58$ kV/cm), respectively. For the radiative lifetime, we expect the opposite voltage dependence since the increasing separation of electron and hole reduces their wave function overlap. This is confirmed by calculations of the radiative lifetime of spatially indirect excitons as a function of F for a realistic QP morphology using a strain-dependent 8-band $k \cdot p$ model.[15,16,20] They are shown by the black line in Figure 3b and for a larger range of F in Supporting Information Figure S3. However, the observed lifetime shortening is well-explained by a reduction of the tunnelling time between the confined QP states and the GaAs matrix schematically shown in Figure 3a. In a simple model, the tunnelling time ($t_{tunnelling}$) can be described by a one-dimensional *WKB* approximation (Fowler−Nordheim tunnelling) given by

$$1/t_{tunnelling} = \frac{\hbar\pi}{2m_e^* L^2} \cdot \exp\left[\frac{-4}{3\hbar eF}\sqrt{2m_e^* E_{ion}^3}\right] \qquad (1)$$

Here, m_e^*, L, and E_{ion} are the electron effective mass, the length of the confinement potential, and the ionization energy, respectively. We assume that electron tunnelling is faster than that of holes because of their smaller effective mass[21] and compare in Figure 3b $t_{tunnelling}$ (red line) with the experimentally measured decay times. The experimental data is well-reproduced by this model using $m_e^* = 0.062 m_0$ and $E_{ion} = 170$ meV which are in good agreement with our calculations and PL data.[15,16] The radiative contribution shows the opposite behavior as the tunnelling process and decreases with increasing field because of a reduction in the electron−hole overlap. At ~50 kV/cm, the time scales for tunnelling and radiative losses are comparable giving rise to the maximum storage times of 50 ms. Since our experimental data is reproduced by the computed behavior for tunnel escape of electrons, we conclude that this process is the dominant loss mechanism in this field range. Clearly, the storage time could be further increased to seconds, limited only by radiative decay (Figure S3) by suppressing tunnel escape with a higher bandgap material like AlGaAs for capping the QPs.

In a final experiment, we investigated the temporal statistics of the storage signal. By moving our detection time

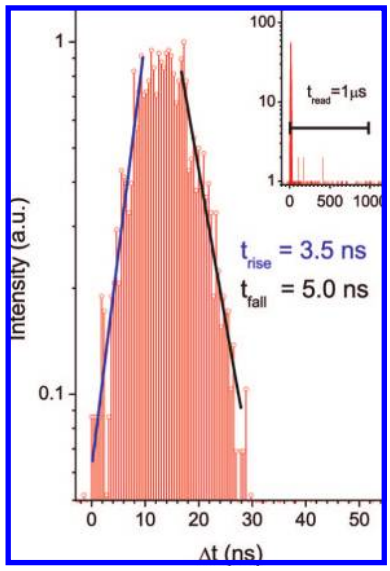

Figure 4. Fast exciton−photon reconversion. In the time-resolved storage signal, photons are detected in a short window after the read voltage is applied (see inset). The stored excitons are efficiently reconverted into photons within 25 ns after reset much shorter than the 1 μs duration of voltage pulse. The fast rise time of 3.5 ns is limited by the device impedance and demonstrates direct reconversion from excitons into photons and excludes injection of one carrier species from the doped contact layers.

window relative to the sample and laser sequence, we found that the storage signal is only detected during the read voltage pulse as shown in Supporting Information Figure S4. To improve our temporal resolution, we performed a time-correlated single photon counting experiment of the storage signal. In Figure 4, the logarithmic number of detection events is plotted as a function of the delay Δt between the time the read voltage is turned on and the time the reconverted photon is detected. For the storage signal, we find a narrow peak with a width of 15 ns and rise and fall times of $t_{rise} = 3.5$ ns and $t_{fall} = 5.0$ ns, respectively. No more photons are detected afterward over the duration ($t_{read} = 1$ μs) of the read voltage pulse as shown in the inset. We want to note that this fast read-out excludes carrier injection from the doped reservoirs which are separated from the QPs by 110 nm intrinsic GaAs barriers, confirming storage of electrons and holes within the QPs. Moreover, this fast read-out is not possible with conventional QD based schemes, and in our device it is only limited entirely by the *RC* time constant of the device itself. It can be optimized for efficient, fast exciton−photon conversion for quantum information implementations or triggered single photon generation.

Our device and storage scheme provide exactly the desired behavior for applications in coherent and optoelectronic devices since it can be readily extended to purely electrical pumping. Here, carriers are injected electrically from the doped reservoirs under a large forward bias. After fast electrical switching to the storage voltage, radiative recombination is suppressed, and the remaining excitons are stored. We find efficient storage for electrical injection and a comparison of two spectra taken under electrical and optical pumping is shown in Supporting Information Figure S5. This injection scheme could be crucial for a deterministic, electrically pumped single photon source or refreshing of optical phase modulation devices.

In summary, we have demonstrated a novel scheme to store a single exciton in a single QP, without the dephasing transfer of one carrier into a reservoir, as required in a QD based method. Long storage times of more than 30 ms are found which are not limited by radiative recombination and which are not accessible for pairs of QDs since tunnel coupling is required for coherent spin-preserving interdot charge transfer.[10,11,14] By modeling potential physical mechanisms as a function of the applied electric field, we identified a slow tunnelling process of electrons out of the QPs which dominates the loss of the stored excitons. Furthermore, the observed time scales exceed measured relaxation and decoherence times of spins in QDs.[3,4,22] Since both electron and hole are kept in the memory, their mutual spin coherence could be probed directly and without the limitation of a short radiative lifetime. For further detailed studies on individual QPs, our device can be combined with optical cavities to increase light extraction[23,24] and significantly improve the signal/noise ratio in these delicate experiments. Since our scheme preserves phase information, it could provide a direct route to convert stationary (spin or exciton) into flying (photon) qBITs.[19] This would open a whole field of experiments and novel concepts for implementing optical and electrical quantum computation schemes. To ensure this a resonant[3] pumping scheme of the optically active direct exciton preferentially using π pulses[5] is required to prevent charged and multiexcitonic contributions. This could be achieved by reducing the device capacitance by shrinking its dimensions to allow for faster switching. With such a device, the electric field can be switched to storage conditions after the exciton is generated using a resonant optical pulse before radiative decay can take place. The electrostatic dipole moments of the optically or electrically generated and stored indirect excitons exceed those of single or coupled QDs by several orders of magnitude and are well suited for applications in electro-optical devices with superior performance.[25]

Acknowledgment. This work was supported by NSF via Nanoscale Interdisciplinary Research Team Grant CCF-0507295 and NSEC-Harvard. H.J.K. acknowledges support by the Alexander-von-Humboldt-Foundation. We thank M. T. Rakher for help with the autocorrelation measurements.

Supporting Information Available: Description of sample growth, device design, and fabrication, with six supporting figures. This material is available free of charge via the Internet at http://pubs.acs.org.

References

(1) Bhattacharya, P.; Ghosh, S; Stiff-Roberts, A. D. *Annu. Rev. Mater. Res.* **2004**, *34*, 1.
(2) Hanson, R.; Kouwenhoven; L. P.; Petta, J. R.; Tarucha, S.; Vandersypen, L. M. K. *Rev. Mod. Phys.* **2007**, *79*, 1217.
(3) Kroutvar, M.; Ducommun, Y.; Heiss, D.; Schuh, D.; Bichler, M.; Abstreiter, G.; Finley, J. J. *Nature* **2004**, *432*, 81–84.
(4) Greilich, A.; Yakovlev, D. R.; Shabaev, A.; Efros, Al. L.; Yugova, I. A.; Oulton, R.; Stavarache, V.; Reuter, D.; Wieck, A.; Bayer, M. *Science* **2006**, *313*, 341–345.
(5) Zrenner A.; Beham, E.; Stufler, S; Findeis, F.; Bichler, M.; Abstreiter, G. *Nature* **2002**, *418*, 612–614.

(6) Xu, X.; Sun, B.; Berman, P. R.; Steel, D. G.; Bracker, A. S.; Gammon, D.; Sham, L. J. *Science* **2007**, *317*, 929–932.
(7) Michler, P.; Kiraz, A.; Becher, C.; Schoenfeld, W. V.; Petroff, P. M.; Zhang, L.; Hu, E.; Imamoglu, A. *Science* **2000**, *290*, 2282–2285.
(8) Akopian, N.; Poem, E.; Berlatzky, J. A.; Avron, J.; Gershoni, D.; Gerardot, B. D.; Petroff, P. M. *Phys. Rev. Lett.* **2006**, *96*, 130501.
(9) Cerletti, V.; Coish, W. A.; Gywat, O.; Loss, D. *Nanotechnology* **2005**, *16*, R27−R49.
(10) Krenner, H. J.; Sabathil, M.; Clark, E. C.; Kress, A.; Schuh, D.; Bichler, M.; Abstreiter, G.; Finley, J. J. *Phys. Rev. Lett.* **2005**, *94*, 57402.
(11) Stinaff, E. A.; Scheibner, M.; Bracker, A. S.; Ponomarev, I. V.; Korenev, V. L.; Ware, M. E.; Doty, M. F.; Reinecke, T. L.; Gammon, D. *Science* **2006**, *311*, 636–639.
(12) Stufler, S.; Ester, P.; Zrenner, A. Bichler, M. *Phys. Rev. Lett.* **2006**, *96*, 037402.
(13) Finley, J. J.; Skalitz, M.; Arzberger, M.; Zrenner, A.; Böhm, G.; Abstreiter, G. *Appl. Phys. Lett.* **1998**, *73*, 2618–2620.
(14) Lundstrom, T.; Schoenfeld, W.; Lee, H.; Petroff, P. M. *Science* **1999**, *286*, 2312–2314.
(15) He, J.; Krenner, H. J.; Pryor, C.; Zhang, J. P.; Wu, Y.; Allen, D. G.; Morris, C. M.; Sherwin, M. S.; Petroff, P. M. *Nano Lett.* **2007**, *7*, 802–806.
(16) Krenner, H. J.; Pryor, C.; He, J; Zhang, J. P.; Wu, Y.; Morris, C. M.; Sherwin, M. S.; Petroff, P. M. *Physica E* **2008**, *40*, 1785–1789.
(17) Polland, H.-J.; Schultheis, L.; Kuhl, J.; Göbel, E. O.; Tu, C. W. *Phys. Rev. Lett.* **1985**, *55*, 2610.
(18) Golub, J. E.; Kash, K.; Harbison, J. P.; Florez, L. T. *Phys. Rev. B* **1990**, *41*, 8564–8567.
(19) Cirac, J. I.; Zoller, P.; Kimble, H. J.; Mabuchi, H. *Phys. Rev. Lett.* **1997**, *78*, 3221–3224.
(20) Pryor, C. *Phys. Rev. B* **1998**, *57*, 7190–7195.
(21) Fry, P. W.; Finley, J. J.; Wilson, L. R.; Lemaitre, A.; Mowbray, D. J.; Skolnick, M. S.; Hopkinson, M.; Hill, G.; Clark, J. C. *Appl. Phys. Lett.* **2000**, *77*, 4344–4346.
(22) Gerardot, B. D.; Brunner, D.; Dalgarno, P. A.; Öhberg, P.; Seidl, S.; Kroner, M.; Karrai, K.; Stoltz, N. G.; Petroff, P. M.; Warburton, R. J. *Nature* **2008**, *451*, 441.
(23) Badolato, A.; Hennessy, K.; Atatüre, M.; Dreiser, J.; Hu, E.; Petroff, P. M.; Imamoglu, A. *Science* **2005**, *308*, 1158–1116.
(24) Stoltz, N. G.; Rakher, M. T.; Strauf, S.; Badolato, A.; Loftgreen, D. D.; Petroff, P. M.; Coldren, L. A.; Bouwmeester, D. *Appl. Phys. Lett.* **2005**, *87*, 031105.
(25) Moreau, G.; Martinez, A.; Cong, D. Y.; Merghem, K.; Miard, A.; Lemaître, A.; Voisin, P.; Ramdane, P.; Krestnikov, I.; Kovsh, A. R.; Fischer, M.; Koeth, J. *Appl. Phys. Lett.* **2007**, *91*, 091118.

NL800911N